Journal of
Materials Chemistry C

COMMUNICATION

View Article Online
View Journal | View Issue

Cite this: J. Mater. Chem. C, 2015, 3, 3252

Received 30th January 2015,
Accepted 3rd March 2015

DOI: 10.1039/c5tc00296f

www.rsc.org/MaterialsC

On-surface assembly of low-dimensional Pb-coordinated metal–organic structures†

Guoqing Lyu,[a] Ran Zhang,[a] Xin Zhang,[b] Pei Nian Liu*[b] and Nian Lin*[a]

Novel low-dimensional metal–organic structures incorporating heavy metal Pb atoms as coordination centres are formed on a Au(111) surface by means of on-surface metallo-supramolecular assembly. The molecular building blocks are porphyrin derivatives functionalized with pyridyl groups. These building blocks are linked *via* a unique pyridyl–Pb–pyridyl coordination motif that does not exist in conventional coordination chemistry but emerges on the surface. The Pb atoms are coordinated in structures of distinctive morphologies, including one-dimensional single chains, double-chains and ladders, and two-dimensional porous networks, owing to the specific sites of the pyridyl groups in the molecular building blocks.

Introduction

Metal–organic frameworks (MOFs) incorporating p-block metals are very rare in contrast to the abundantly reported d- or f-block metal coordinated MOFs. Pb, as a heavy p-block element, has a large radius, versatile stereochemical activities and a flexible coordination environment.[1–3] These characteristics provide opportunities for constructing Pb-based MOFs that exhibit rich structural topologies and diverse coordination geometries.[4–11] Moreover, the unique electronic configuration of Pb makes the Pb-based MOFs potential electroluminescent devices, light-emitting diodes and fluorescent sensors.[9–11] Recently, it was demonstrated theoretically that a Pb-based two-dimensional (2D) organometallic structure exhibits a non-trivial quantum state, known as the topological insulator phase, due to the strong spin–orbit coupling effects of the heavy Pb atoms.[12] This prediction hints that the Pb-coordinated 2D metal–organic structures may represent a new family of functional materials with appealing electronic and spintronic properties. Experimental realization of these predicated structures is therefore highly desirable.

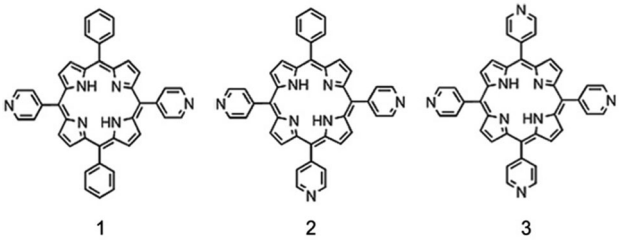

Scheme 1 Chemical structures of the porphyrin derivatives used in this study: 5,15-dipyridyl-10,20-diphenyl-porphyrin (**1**), 5,10,15-tri(4-pyridyl)-20-phenylporphyrin (**2**) and 5,10,15,20-tetra(4-pyridyl)-porphyrin (**3**).

Supramolecular coordination self-assembly taking place at solid–vacuum interfaces is a powerful tool for designing 2D MOFs.[13–16] To date, the 2D MOFs have been mainly constructed with alkali, transition and rare earth, *i.e.*, s-,[17–20] d-,[21–28] and f-block[29–31] metals, while the main group p-block metals remain unexplored. Here we report the self-assembly of Pb-coordinated metal–organic structures on a Au(111) surface. We used three pyridyl functionalized porphyrin derivatives (Scheme 1) as molecular building blocks to coordinate with Pb. We found that Pb is coordinated in a two-fold pyridyl–Pb–pyridyl motif, which resembles the previously reported pyridyl–Cu–pyridyl bonding motif.[32,33] We observed that Pb assembles with **1** to form single-row chains, with **2** to form double-row chains and ladders and with **3** to form two types of porous 2D networks exhibiting rhombus and Kagome lattices, and a multiple-row structure. To our knowledge, this is the first report of on-surface assembled metal–organic structures based on Pb coordination. We also investigated the assembly pathway and thermal stability of these structures and found that the Pb-coordinated bonds are weaker than the Cu-coordinated counterparts, presumably due to their p-block chemistry.

Results and discussion

Fig. 1 is a scanning tunneling microscopy (STM) topograph showing a mixture of **1** and Pb on the Au(111) surface. **1** was

[a] Department of Physics, The Hong Kong University of Science and Technology, Clear Water Bay, Hong Kong, China. E-mail: phnlin@ust.hk
[b] Shanghai Key Laboratory of Functional Materials Chemistry and Institute of Fine Chemicals, East China University of Science and Technology, Meilong Road 130, Shanghai, China. E-mail: liupn@ecust.edu.cn

† Electronic supplementary information (ESI) available. See DOI: 10.1039/c5tc00296f

deposited first and Pb atoms were deposited later on the sample. During the deposition, the sample was held at room temperature. Without Pb, **1** was in a highly mobile 2D gas phase on the surface. The hexagonal-shaped islands shown in Fig. 1 are Pb islands. The molecules form two structures. Most molecules aggregated as closely packed islands (blue arrow) and a small portion of the molecules forms chains (white arrow). The top-left inset in Fig. 1 is a magnified image of the closely packed molecule islands with a molecular model overlaid. This structure can be rationalized by inter-molecular hydrogen bonds arising from the periphery pyridyl functional groups, as highlighted by the dashed lines in the model (see detailed description and discussion in the ESI†).

The chains are composed of a single-row of molecules, denoted as **SR** chains thereafter. Note that the **SR** chains often terminate at a Pb island or a molecule island. Many **SR** chains are not perfectly straight but exhibit a curved morphology. The **SR** chains frequently changed their morphology during STM scanning, indicating that the **SR** chains were mobile. These phenomena reflect flexibility of the inter-molecular bonding in the **SR** chains. The distance between the neighboring molecules in the **SR** chains is 1.92 ± 0.05 nm. Similar chain structures were observed in the self-assembly of **1** and Cu on Au(111) and were confirmed to be metal–organic chains with a pyridyl–Cu–pyridyl bonding motif.[33] We attribute the **SR** chains to a similar structure that is stabilized by two-fold pyridyl–Pb–pyridyl coordination, as illustrated in the structural model in the bottom-right inset in Fig. 1. Despite their distinctive bonding configuration in three-dimensional space, Cu and Pb may be coordinated in similar bonding motifs on a surface, suggesting that the surface alters the intrinsic properties of the adsorbed metal atoms. Assuming that the Pb atom is located at the middle of the two N atoms of the opposing pyridyl groups, the Pb–N bond length is estimated to be 0.20 ± 0.02 nm. This length becomes larger if the Pb atom is not co-planar with the two N atoms or the porphyrin molecules slightly rotate azimuthally. Pb(II) coordination with N-donor ligands such as 2,2′-bipyridine and 4,4′-bipyridine ligands has been reported in solution phase complexes,[34–36] which feature a Pb–N bond length in the range of 0.24 to 0.26 nm. The bond length of the on-surface Pb–N coordination is thus comparable with the typical Pb–N bond length in the solution phase complexes.

Annealing the sample to 100–150 °C reduced the amounts of **SR** chains and shortened their length, in the mean time increased the size of the closely packed molecule islands. Annealing the sample above 150 °C caused the **SR** chains to disappear entirely and all molecules aggregated as molecule islands while Pb atoms form big Pb islands. These phenomena indicate that the **SR** chains are kinetically controlled products. Presumably, the on-surface pyridyl–Pb–pyridyl coordination is of moderate bond strength, as a result, the free energy of the **SR** chains is higher than that of a system consisting of the closely packed molecule islands and the Pb islands.

2 deposited on Au(111) was in a highly mobile 2D gas phase too. After dosing Pb atoms on this sample held at room temperature, closely packed molecule islands appeared. Annealing the sample at 140 °C induced the formation of line structures (Fig. 2a). The lines are very long, with some extending over 400 nm, and feature kinks, right-angle turns and T-shape joints (see ESI†). Fig. 2b shows a magnified view of a line with a kink. The line is made out of double rows of molecules (denoted as **DR**). Two neighboring rows are interlocked in a zigzag manner with a row-to-row distance of 1.14 ± 0.05 nm. A structural model of the **DR** structure is shown in Fig. 2c: the molecules are linked *via* pyridyl–Pb–pyridyl coordination along the rows. Within a row, the neighboring molecules are 1.82 nm

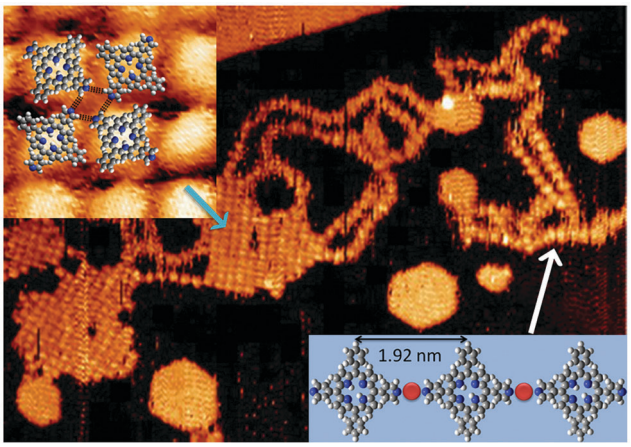

Fig. 1 An overview STM topograph showing **1** and Pb forming **SR** chains (100 × 70 nm^2). (top-left inset) Magnified view of a closely packed network (4 × 4 nm^2) with a tentative model overlaid. The dashed lines indicate hydrogen bonds. (bottom-right inset) Structural model of the **SR** chain. Color codes: C, gray; N, blue; H, white; Pb, red.

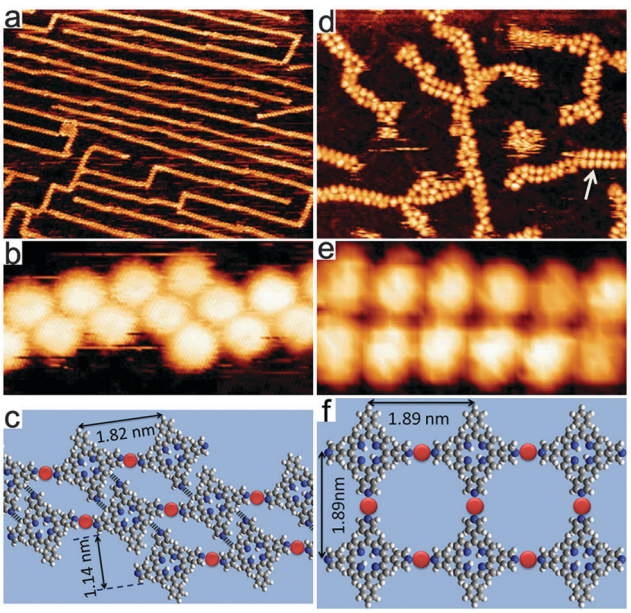

Fig. 2 (a) and (d) STM topographs showing **DR** chains and the ladder structures formed out of **2** and Pb (113 × 151 nm^2 and 54 × 72 nm^2), respectively. (b) and (e) High-resolution images of a **DR** chain and a ladder structure (5 × 10 nm^2). (c) and (f) Structural models of the **DR** chain and the ladder structure, respectively. The dashed lines indicate hydrogen bonds.

apart, which is 0.1 nm closer than those in an **SR** chain. To attain a reasonable Pb–N distance, we propose that the molecules in the **DR** chains turn azimuthally. As shown in the model (Fig. 2c), the molecules rotate 8° off the long axes of the row, resulting in a 0.20 ± 0.02 nm Pb–N distance. The model also shows that the N atom of the *ortho*-pyridyl group approaches the H atom at a *beta*-position of the porphyrin moiety of the molecule in the adjacent row. The N–H distance is 0.20 ± 0.02 nm (dashed line), which may invoke an inter-molecular hydrogen bond. Such hydrogen bonds inter-link two rows into the **DR** structure. At the kink, a molecule flips upside down to form hydrogen bonds with the molecule(s) in the top row and the molecule(s) in the bottom row. One possible scenario is illustrated in Fig. 2c.

Dosing additional amount of Pb on this sample and annealing at 170 °C formed a ladder structure (Fig. 2d, white arrow) alongside the **DR** chains. The ladders are shorter than the **DR** chains, typically consisting of less than 10 dimer units. As shown in a high-resolution STM image of a ladder (Fig. 2e), each molecule links to three neighboring ones at a distance of 1.89 ± 0.05 nm. We propose that in this structure all three pyridyl groups participate in pyridyl–Pb–pyridyl coordination (Fig. 2f).[37] The ladder structures are less stable than the **DR** chains, as evidenced by the structural changes occurred during STM scanning. Moreover, after annealing the sample at 200 °C, the ladders disappeared but the **DR** chains remained. The thermal stability of the **DR** and ladder structures will be discussed later.

Depositing Pb first and **3** later on Au(111), or simultaneous deposition of the two components, generated closely packed molecule islands and Pb islands, but no coordination structures (see ESI†). To form well-ordered coordination structures, **3** was deposited on the surface first, and Pb atoms were deposited later onto the sample which was held at 60–120 °C. Fig. 3a displays two types of porous networks, exhibiting a Kagome lattice and a rhombus lattice, respectively, alongside small patches of closely packed molecule islands. The Kagome networks grew on open terraces with a typical domain size of 30–50 nm. The rhombus networks are smaller, with a typical domain size below 20 nm, and always connected with the closely packed molecule islands. Fig. 3b shows a high resolution STM image of the Kagome structure. One can see that each molecule is attached to four neighboring ones, whereas three molecules form a symmetric three-branch joint, thus constructing a Kagome lattice.[26] The diameter of the hexagon is 3.63 ± 0.05 nm. Fig. 3d shows a model of the Kagome structure with a Pb–N distance of 0.20 ± 0.02 nm. Fig. 3c shows a high-resolution STM image of the rhombus structure. The rhombus has two corners at 85° and two corners at 95°. This deviation from a perfect square structure is attributed to the symmetry mismatch between the network and the substrate.[38,39] The side of the rhombus structure is 1.92 ± 0.05 nm long, featuring a Pb–N bond length of 0.20 ± 0.02 nm. Fig. 3e shows a model of the rhombus structure.

Annealing this sample at 160 °C destroyed both porous network structures and formed a new structure. As shown in Fig. 4a, the molecules **3** formed 2D islands as large as ~100 nm. The islands always ended at mono-atomic steps of the Au(111) surface and have two straight edges, implying that

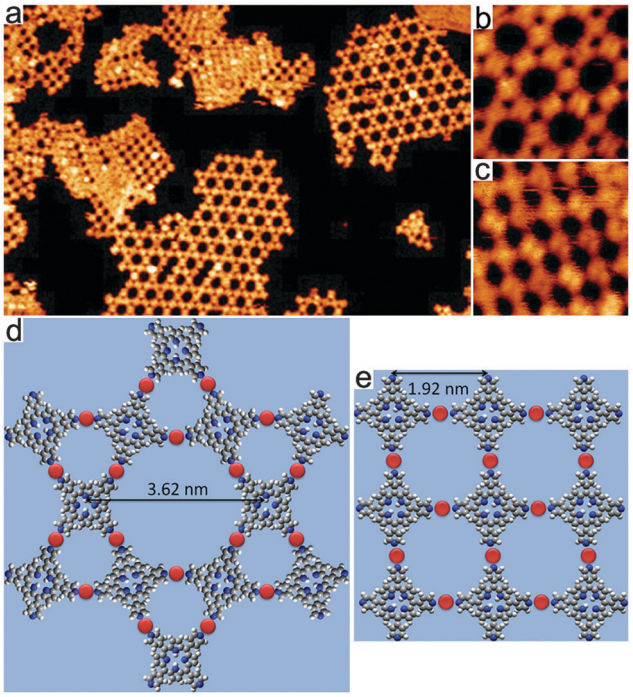

Fig. 3 (a) STM topograph showing **3** and Pb forming close-packed islands, Kagome and rhombus porous networks (90 × 60 nm^2). (b) and (c) High-resolution images of the Kagome and rhombus networks (12 × 12 nm^2). (d) and (e) Structural models of the Kagome and rhombus networks.

the inter-molecular interaction is different along the two orthogonal directions in the islands. Close inspection revealed that the islands contain rows of holes. A magnified STM topograph (Fig. 4b) shows that the 2D island consists of multiple parallel molecule rows (denoted as **MR**), as highlighted by the black arrow lines. Along the rows, the molecules arrange with an inter-molecular distance of 1.89 ± 0.05 nm. The adjacent rows are packed with a row-to-row distance of 1.15 ± 0.05 nm. This structure is thus similar to the **DR** structure. We propose that the bonding configuration in the **MR** structure resembles the **DR** chains, that is, pyridyl–Pb–pyridyl coordination along each row and hydrogen bonding between the adjacent rows, as illustrated by the structural model in Fig. 4c. The arrows define the clockwise or counter clockwise azimuth rotation of the molecules with respect to the row axes. As the two adjacent rows are made out of oppositely rotating molecules, larger voids appear between the two rows, accounting for the holes in the STM topograph.

The six Pb-coordinated structures were assembled under specific conditions and exhibited different thermal stabilities, as summarized in Table 1. To form the **SR** structure, **1** was first deposited on the surface and subsequently Pb atoms were dosed to the sample at room temperature. Reversing the deposition sequence or simultaneous deposition of the two components did not result in the **SR** structure. Annealing the sample at 150 °C and cooling to 30 °C dissolved the **SR** structure. This behaviour hints that the self-assembly of the **SR** structure is a kinetically controlled process. In contrast, self-assembly of the **DR** structure required high-temperature annealing of the mixture of **2** and Pb,

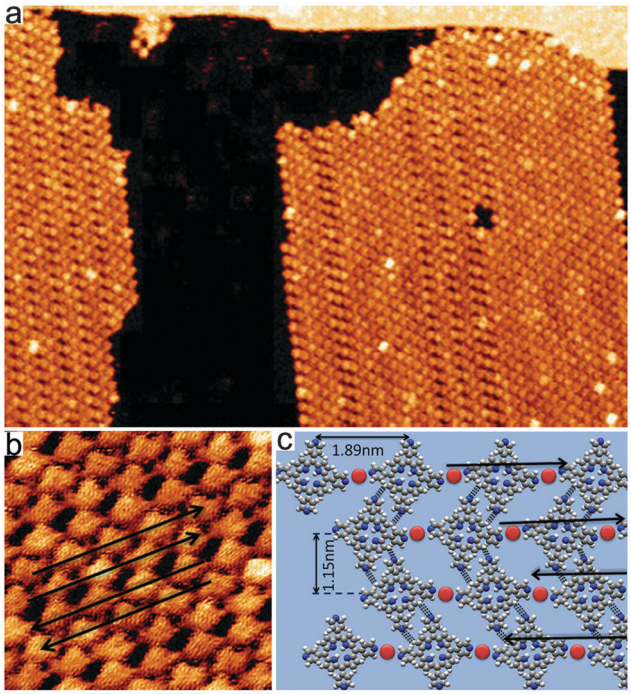

Fig. 4 (a) An overview STM topograph of the **MR** structure (90 × 60 nm^2). (b) High-resolution image (10 nm × 10 nm^2). The arrows highlight the rows. (c) Structural model of the **MR** structure. The dashed lines indicate hydrogen bonds. The arrow direction indicates the azimuth rotation of the molecules in that row.

so this process is thermodynamically controlled. The ladder structure, however, formed at a moderate annealing temperature of 170 °C and dissolved after annealing at 200 °C. Thus the assembly of the ladder structure is a process ruled by both kinetic and thermodynamic control. The self-assembly of the porous networks is most intriguing. It took place under the conditions of (1) **3** must be deposited on the surface first; (2) Pb atoms were dosed to the sample which was held at 60–120 °C; (3) the dosing flux of Pb was kept very low, 0.02 ML min^{-1}. Deviation from these optimized conditions reduced the network size and more molecules were incorporated into the closely packed molecule islands. Moreover, annealing treatment did not enlarge but rather reduced the network domain size. The porous networks dissolved upon annealing at 160 °C, thus, are kinetic products. The **MR** structure, in contrast, remained stable even after annealing at 240 °C. Apparently, this structure is a thermodynamic product. Note that among the five structures, two thermodynamic products of the **DR** and **MR** structures can be assembled by dissolving Pb islands using high-temperature annealing in the presence of the corresponding molecules.

The differences in the self-assembly behaviours and thermal stability can be partially rationalized in terms of inter-molecular bond energy. The number of bonds per molecule in each structure is listed in Table 1. Among the five structures, those stabilized purely by coordination bonds are kinetically controlled structures, while those stabilized by a combination of coordination and hydrogen bonds are the thermodynamically stable ones. The **MR** structure, which has two coordination bonds and two hydrogen bonds per molecule, is more stable than the porous network structures which have four coordination bonds per molecule. Likewise, the **DR** structure, which has two coordination bonds and one hydrogen bond per molecule, is more stable than the ladder structure, which has three coordination bonds per molecule. We propose that the surface-stabilized pyridyl–Pb–pyridyl coordination is of moderate strength, which is comparable to or even weaker than the inter-molecular hydrogen bonds. Therefore the thermal stability of these structures can be correlated with the average bond energy per molecule.

Conclusions

In summary, we have investigated the self-assembly of Pb with a series of pyridyl-functionalized porphyrin derivatives. A two-fold pyridyl–Pb–pyridyl coordination motif articulates the molecular building blocks into metal–organic structures. The number and positions of the pyridyl groups on the porphyrin moiety control the dimensionality of the metal–organic structures, ranging from one-dimensional (single-row chains), quasi 2D (ladders) to 2D (porous networks). The structures involving coordination

Table 1 Summary of the structures formed in this study and their assembly conditions

Molecule	**1**	**2**		**3**	
Structure	**SR**	**DR**	Ladder	Porous networks[b]	MR
Deposition sequence	(1) **1**; (2) Pb	Arbitrary	Arbitrary	(1) **1**; (2) Pb	Arbitrary
Assembly temperature	30–100 °C	140–180 °C	170 °C	60–120 °C	200–240 °C
Assembly path	Kinetic	Thermodynamic	Kinetic	Kinetic	Thermodynamic
Thermal stability	Low	High	Moderate	Moderate	Highest
Model			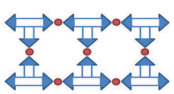	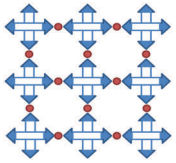	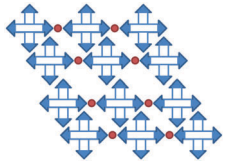
No. of bonds[a] per molecule	2C	2C + 1H	3C	4C	2C + 2H

[a] C stands for the coordination bond and H stands for the hydrogen bond. [b] As the Kagome and the rhombus networks exhibit similar self-assembly and structural characteristics, these two structures are categorized as porous networks and represented by the model of a square network.

bonds only are metastable kinetic products, whereas the structures involving a combined coordination and hydrogen bonds are thermodynamic products. These features imply that the p-block chemistry of Pb results in relatively weak pyridyl–Pb–pyridyl coordination as compared with those incorporating d-block elements. The physical and chemical properties of these structures including the oxidation state of the Pb atoms deserve further studies. The structures reported here are in close contact with the Au surface, which might significantly alter their electronic, in particular the non-trivial topological, properties. To realize the structures that resemble the free-standing 2D organic topological insulating layers presented in ref. 12, it is highly desirable to produce these structures on an insulating substrate.

Experimental section

All the experiments were conducted using an ultrahigh-vacuum system (Omicron Nanotechnology) with a base pressure of 3×10^{-10} mbar. A single-crystalline Au(111) substrate was cleaned by repeated cycles of Ar^+ sputtering and annealing to about 620 °C afterwards. The molecules **1**, **2**, and **3** were evaporated at 320 °C, 340 °C, and 355 °C, respectively, and deposited onto the Au(111) surface held at room temperature. Pb atoms were dosed onto the Au(111) surface using an electron-beam evaporator. The samples were characterized using a scanning tunneling microscope operated at room temperature in a constant current mode with a tunneling current of 0.3 nA and bias voltage of −1.1 V. **1** and **2** were synthesized[37] and **3** was purchased from Sigma Aldrich.

Acknowledgements

This work was supported by Hong Kong RGC 16303514, the National Natural Science Foundation of China (Project No. 21172069, 21372072 and 21190033) and the Science Fund for Creative Research Groups (21421004).

Notes and references

1 P. Pyykk, *Chem. Rev.*, 1988, **88**, 563–594.
2 J. M. Harrowfield, H. Miyamae, B. W. Skelton, A. A. Soudi and A. H. White, *Aust. J. Chem.*, 1996, **49**, 1165–1169.
3 L. Shimoni-Livny, J. P. Glusker and C. W. Brock, *Inorg. Chem.*, 1998, **37**, 1853–1867.
4 E. C. Yang, J. Li, B. Ding, Q. Q. Liang, X. G. Wang and X. J. Zhao, *CrystEngComm*, 2008, **10**, 158–161.
5 S. R. Fan and L. G. Zhu, *Inorg. Chem.*, 2006, **45**, 7935–7942.
6 B. J. Greer, V. K. Michaelis, M. J. Katz, D. B. Leznoff, G. Schreckenbach and S. Kroeker, *Chem. – Eur. J.*, 2011, **17**, 3609–3618.
7 L. Zhang, Z.-J. Li, Q.-P. Lin, Y.-Y. Qin, J. Zhang, P.-X. Yin, J.-K. Cheng and Y.-G. Yao, *Inorg. Chem.*, 2009, **48**, 6517–6525.
8 J. Yang, J.-F. Ma, Y.-Y. Liu, J.-C. Ma and S. R. Batten, *Inorg. Chem.*, 2007, **46**, 6542–6555.
9 B. Sui, W. Zhao, G. Ma, T. Okamura, J. Fan, Y. Z. Li, S. H. Tang, W. Y. Sun and N. Ueyama, *J. Mater. Chem.*, 2004, **14**, 1631–1639.
10 J. E. H. Buston, T. D. W. Claridge, S. J. Heyes, M. A. Leech, M. G. Moloney and K. Prout, *Dalton Trans.*, 2005, 3195–3203.
11 J.-G. Mao, Z.-K. Wang and A. Clearfield, *Inorg. Chem.*, 2002, **41**, 6106–6111.
12 Z. F. Wang, Z. Liu and F. Liu, *Nat. Commun.*, 2013, **4**, 1471.
13 J. V. Barth, *Annu. Rev. Phys. Chem.*, 2007, **58**, 375–407.
14 S. Stepanow, N. Lin and J. V. Barth, *J. Phys.: Condens. Matter*, 2008, **20**, 184002.
15 N. Lin, S. Stepanow, M. Ruben and J. V. Barth, *Top. Curr. Chem.*, 2009, **287**, 1–44.
16 H. Liang, Y. He, Y. Ye, X. Xu, F. Cheng, W. Sun, X. Shao, Y. Wang, J. Li and K. Wu, *Coord. Chem. Rev.*, 2009, **253**, 2959–2979.
17 S. Stepanow, R. Ohmann, F. Leroy, N. Lin, T. Strunskus, C. Wöll and K. Kern, *ACS Nano*, 2010, **4**, 1813–1820.
18 C. Wäckerlin, C. Iacovita, D. Chylarecka, P. Fesser, T. A. Jung and N. Ballav, *Chem. Commun.*, 2011, **47**, 9146–9148.
19 D. Skomski, S. Abb and S. L. Tait, *J. Am. Chem. Soc.*, 2012, **134**, 14165–14171.
20 N. Abdurakhmanova, A. Floris, T.-C. Tseng, A. Comisso, S. Stepanow, A. De Vita and K. Kern, *Nat. Commun.*, 2012, **3**, 940.
21 A. Dmitriev, H. Spillmann, N. Lin, J. V. Barth and K. Kern, *Angew. Chem., Int. Ed.*, 2003, **42**, 2670–2673.
22 S. Stepanow, N. Lin, D. Payer, U. Schlickum, F. Klappenberger, G. Zoppellaro, M. Ruben, H. Brune, J. V. Barth and K. Kern, *Angew. Chem., Int. Ed.*, 2007, **46**, 710–713.
23 S. L. Tait, A. Langner, N. Lin, R. Chandrasekar, M. Ruben and K. Kern, *ChemPhysChem*, 2008, **9**, 2495–2499.
24 T.-C. Tseng, C. Lin, X. Shi, S. L. Tait, X. Liu, U. Starke, N. Lin, R. Zhang, C. Minot, M. A. Van Hove, J. I. Cerdá and K. Kern, *Phys. Rev. B: Condens. Matter Mater. Phys.*, 2009, **80**, 155458.
25 J. Čechal, C. S. Kley, T. Kumagai, F. Schramm, M. Ruben, S. Stepanow and K. Kern, *Chem. Commun.*, 2014, **50**, 9973–9976.
26 Z. Shi and N. Lin, *J. Am. Chem. Soc.*, 2009, **131**, 5376–5377.
27 D. Skomski, C. D. Tempas, G. S. Bukowski, K. A. Smith and S. L. Tait, *J. Chem. Phys.*, 2015, **142**, 101913.
28 D. Skomski, C. D. Tempas, K. A. Smith and S. L. Tait, *J. Am. Chem. Soc.*, 2014, **136**, 9862–9865.
29 J. I. Urgel, D. Ecija, W. Auwärter, A. C. Papageorgiou, A. P. Seitsonen, S. Vijayaraghavan, S. Joshi, S. Fischer, J. Reichert and J. V. Barth, *J. Phys. Chem. C*, 2014, **118**, 12908–12915.
30 J. I. Urgel, D. Ecija, W. Auwärter and J. V. Barth, *Nano Lett.*, 2014, **14**, 1369–1373.
31 D. Ecija, J. I. Urgel, A. C. Papageorgiou, S. Joshi, W. Auwärter, A. P. Seitsonen, S. Klyatskaya, M. Ruben, S. Fischer, S. Vijayaraghavan, J. Reichert and J. V. Barth, *Proc. Natl. Acad. Sci. U. S. A.*, 2013, **110**, 6678–6681.
32 S. L. Tait, A. Langner, N. Lin, S. Stepanow, C. Rajadurai, M. Ruben and K. Kern, *J. Phys. Chem. C*, 2007, **111**, 10982–10987.
33 T. Lin, X. S. Shang, J. Adisoejoso, P. N. Liu and N. Lin, *J. Am. Chem. Soc.*, 2013, **135**, 3576–3582.

34 A. Morsali, M. Payeghader, S. S. Monfared and M. Moradi, *J. Coord. Chem.*, 2003, **56**, 761–770.
35 A. Morsali and X.-M. Chen, *J. Coord. Chem.*, 2004, **57**, 1233–1241.
36 K. J. Nordell, K. N. Schultz, K. A. Higgins and M. D. Smith, *Polyhedron*, 2004, **23**, 2161–2167.
37 J. Adisoejoso, Y. Li, J. Liu, P. N. Liu and N. Lin, *J. Am. Chem. Soc.*, 2012, **134**, 18526–18529.
38 Z. Shi and N. Lin, *ChemPhysChem*, 2010, **11**, 97–100.
39 Y. Li, J. Xiao, T. Shubina, M. Chen, Z. Shi, M. Schmid, H.-P. Steinrueck, M. Gottfried and N. Lin, *J. Am. Chem. Soc.*, 2012, **134**, 6401–6408.